HEFAT2008
6th International Conference on Heat Transfer, Fluid Mechanics and Thermodynamics
30 June to 2 July 2008
Pretoria, South Africa
Paper number: CM1

SIMULTANEOUS LAMINAR NATURAL CONVECTION ABOVE AND BELOW TILTED THIN PLATES

C. Cianfrini[a], M. Corcione [a,]*, A. D'Orazio[b] and E. Habib[a]
*Author for correspondence
[a]Dipartimento di Fisica Tecnica, "Sapienza" University of Rome
via Eudossiana, 18 – 00184 Rome, Italy
[b]Dipartimento di Meccanica e Aeronautica, "Sapienza" University of Rome
via Eudossiana, 18 – 00184 Rome, Italy
e-mail: massimo.corcione@uniroma1.it

ABSTRACT

Steady laminar natural convection heat transfer from tilted thin plates with both sides heated at uniform temperature, is studied numerically. A computer code based on the SIMPLE-C algorithm is used for the solution of the mass, momentum, and energy conservation equations. Simulations are performed for different values of the inclination angle of the plate in the range between 0deg and 75deg, the Rayleigh number in the range between 10^1 and 10^8, and the Prandtl number in the range between 0.7 and 70, whose effects on the flow and temperature fields, and on the heat transfer rate, are analyzed in detail. In addition, comparisons with the case of heating at a single side of the plate are executed and discussed.

INTRODUCTION

Convection induced by buoyancy above or below a finite-size heated plate of arbitrary inclination is one of the basic classic problems in free convection heat transfer, as it appears in a number of engineering applications, as well as in several natural circumstances.

Experimental studies on either upward or downward facing inclined plates were performed by Kierkus [1], Hassan and Mohamed [2], Fujii and Imura [3], and Al-Arabi and Sakr [4], for the case of uniform wall temperature, and by Vliet [5], Vliet and Ross [6], Fussey and Warneford [7], Shaukatullah and Gebhart [8], and King and Reible [9], for the case of uniform heat flux. The working fluids were either air – used in [1], [2], [4], and [6] – or water – used in [3], [5], [7], [8], and [9]. The results were reported in terms of either the average Nusselt number – in [3], [4], [8], and [9] – or the local Nusselt number – in [1], [2], [5], [6], and [7].

Theoretical solutions were obtained by Kierkus [1], and by Hasan and Eichhorn [10], for isothermal surfaces facing both upwards and downwards, as well as by Chen et al. [11], for upward-facing, semi-infinite flat plates in both cases of uniform wall temperature and uniform heat flux.

However, all the above papers deal with plates heated at a single side. In contrast, although in applications the situation in which both sides of the plate are simultaneously heated may occur, a definitely smaller degree of attention has been devoted to this problem, which was treated only by Wei et al. [12], who executed a numerical study under the assumption of uniform heat generation.

In this background, the aim of the present paper is to carry out a study of free convetion from an inclined thin plate whose both sides are heated at uniform temperature, with the scope to highlight in what measure the heat transfer performance of any side of the plate is affected by the simultaneous heating of the opposite side of the plate.

The study is conducted numerically under the assumption of steady, two-dimensional laminar flow. A computer code based on the SIMPLE-C algorithm is employed for the solution of the mass, momentum and energy governing equations. Simulations are performed for different values of the angle of inclination of the plate from 0deg to 75deg, the Rayleigh number from 10^1 to 10^8, and the Prandtl number from 0.7 to 70, whose effects on the flow and temperature fields, as well as on the heat transfer rate, are analyzed in detail and discussed.

PROBLEM FORMULATION

A plate of length L, inclined of an angle φ with respect to gravity, is suspended in free space. The plate thickness d is set at 1/50 of its length. Both sides of the plate are kept at uniform temperature t_p, whereas both ends are assumed to be perfectly insulated. Free convection takes place from the heated sides of the plate to the surrounding undisturbed fluid reservoir, which is assumed at uniform temperature t_∞.

The flow is assumed steady, two-dimensional, laminar, and incompressible, with constant fluid properties and negligible viscous dissipation and pressure work. The buoyancy effects on momentum transfer are taken into account by the Boussinesq approximation.

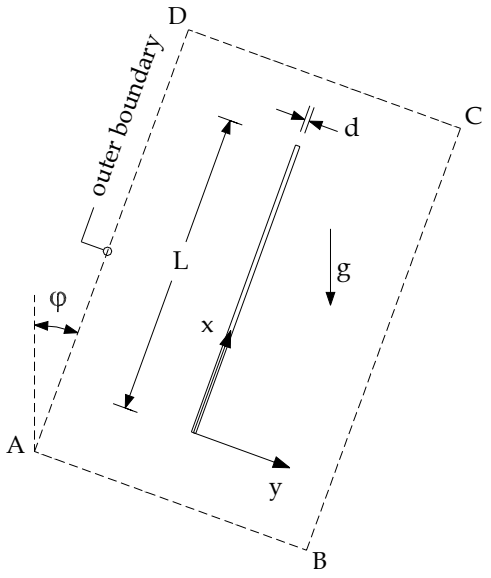

Figure 1 – Geometry, coordinate system and integration domain

Governing equations

Once the above assumptions are used in the conservation equations of mass, momentum and energy, the following set of dimensionless governing equations is obtained:

$$\nabla \cdot \mathbf{V} = 0 \tag{1}$$

$$(\mathbf{V}\cdot\nabla)\mathbf{V} = -\nabla p + \nabla^2 \mathbf{V} - \frac{\mathrm{Ra}}{\mathrm{Pr}} \mathrm{T} \frac{\mathbf{g}}{g} \tag{2}$$

$$(\mathbf{V}\cdot\nabla)\mathrm{T} = \frac{1}{\mathrm{Pr}}\nabla^2 \mathrm{T} \tag{3}$$

where **V** is the dimensionless velocity vector with components U and V parallel and perpendicular to the plate, respectively, normalized with ν/L; T is the dimensionless temperature excess over the temperature of the undisturbed fluid normalized with the temperature difference ($t_p - t_\infty$); p is the dimensionless pressure normalized with $\rho_\infty \nu^2/L^2$; Ra is the Rayleigh number based on the length of the plate; and Pr is the Prandtl number.

Besides the simultaneous heating of both sides of the plate, also the case of heating at a single side (the other side of the plate being adiabatic) is studied for comparison, in order to evaluate how much the heat transfer rate at any side of the plate is affected by the concurrent heating of the opposite side of the plate. Therefore, the boundary conditions are (a) T = 1 and **V** = 0 at any heated side of the plate, (b) $\partial T/\partial n = 0$ and **V** = 0 at any perfectly insulated surface (n denotes the direction normal to the surface), and (c) T = 0 and **V** = 0 at very large distance from the plate.

Computational domain and boundary conditions

The finite-difference solution of equations (1)–(3) with the boundary conditions stated above requires that a computational domain is established. The two-dimensional integration domain is taken as a rectangle which includes the plate and extends sufficiently far from it, as sketched in Fig. 1, in which the (x,y) Cartesian coordinate system adopted is also represented. Such integration domain is filled with a non-uniform grid, having a concentration of grid lines near the plate. As regards the boundary conditions to be assigned at the four lines which enclose the rectangular integration domain, once these lines are set sufficiently far from the plate, the motion of the fluid which enters or leaves the computational domain may reasonably be assumed to occur normally to them. The entering fluid is assumed at the undisturbed free field temperature. In contrast, for the leaving fluid, whose temperature is not known a priori, a zero temperature gradient along the normal to the boundary line is assumed. Accordingly, the following boundary conditions are applied (see Fig. 1):

a) at any heated side of the plate

$$\mathrm{U} = 0\,, \quad \mathrm{V} = 0\,, \quad \mathrm{T} = 1 \tag{4}$$

b) at the insulated side of the plate, when the case of heating at a single side is considered

$$\mathrm{U} = 0\,, \quad \mathrm{V} = 0\,, \quad \frac{\partial \mathrm{T}}{\partial \mathrm{Y}} = 0 \tag{5}$$

c) at both ends of the plate

$$\mathrm{U} = 0\,, \quad \mathrm{V} = 0\,, \quad \frac{\partial \mathrm{T}}{\partial \mathrm{X}} = 0 \tag{6}$$

d) at boundary line A–B

$$\frac{\partial \mathrm{U}}{\partial \mathrm{X}} = 0\,, \quad \mathrm{V} = 0\,, \quad \mathrm{T} = 0 \text{ if } \mathrm{U} \geq 0 \text{ or } \frac{\partial \mathrm{T}}{\partial \mathrm{X}} = 0 \text{ if } \mathrm{U} < 0 \tag{7}$$

e) at boundary line B–C

$$\mathrm{U} = 0\,, \quad \frac{\partial \mathrm{V}}{\partial \mathrm{Y}} = 0\,, \quad \mathrm{T} = 0 \text{ if } \mathrm{V} < 0 \text{ or } \frac{\partial \mathrm{T}}{\partial \mathrm{Y}} = 0 \text{ if } \mathrm{V} \geq 0 \tag{8}$$

f) at boundary line C–D

$$\frac{\partial \mathrm{U}}{\partial \mathrm{X}} = 0\,, \quad \mathrm{V} = 0\,, \quad \mathrm{T} = 0 \text{ if } \mathrm{U} < 0 \text{ or } \frac{\partial \mathrm{T}}{\partial \mathrm{X}} = 0 \text{ if } \mathrm{U} \geq 0 \tag{9}$$

g) at boundary line A–D

$$\mathrm{U} = 0\,, \quad \frac{\partial \mathrm{V}}{\partial \mathrm{Y}} = 0\,, \quad \mathrm{T} = 0 \text{ if } \mathrm{V} \geq 0 \text{ or } \frac{\partial \mathrm{T}}{\partial \mathrm{Y}} = 0 \text{ if } \mathrm{V} < 0 \tag{10}$$

in which X and Y are the dimensionless Cartesian coordinates, normalized with L.

Solution algorithm

The set of equations (1)–(3) with the boundary conditions (4)–(10) is solved numerically by a control-volume formulation of the finite-difference method. The pressure-velocity coupling is handled through the SIMPLE-C algorithm by Van Doormaal and Raithby [13]. The advection fluxes are evaluated by the QUICK discretization scheme by Leonard [14]. Starting from first-approximation distributions of the dependent variables, the

discretized governing equations are solved iteratively via a line-by-line application of the Thomas algorithm, enforcing under-relaxation to ensure convergence. The solution is considered to be converged when the maximum absolute values of the mass source and the percentage changes of the dependent variables at any grid-node between two consecutive iterations are smaller than the prescribed values, i.e., 10^{-4} and 10^{-6}, respectively.

Data reduction

After convergence is attained, the local Nusselt numbers $(Nu_x)_U$ and $(Nu_x)_D$, and the average Nusselt numbers $(Nu)_U$ and $(Nu)_D$, of the upward-facing and downward-facing sides of the plate, respectively, are calculated:

$$(Nu_x)_U = \frac{q_U L}{k(t_p - t_\infty)} = -\left.\frac{\partial T}{\partial Y}\right|_{Y=-d/2L} \tag{11}$$

$$(Nu_x)_D = \frac{q_D L}{k(t_p - t_\infty)} = -\left.\frac{\partial T}{\partial Y}\right|_{Y=+d/2L} \tag{12}$$

$$Nu_U = \frac{Q_U}{k(t_p - t_\infty)} = -\int_0^1 \left(\left.\frac{\partial T}{\partial Y}\right|_{Y=-d/2L}\right) dX \tag{13}$$

$$Nu_D = \frac{Q_D}{k(t_p - t_\infty)} = -\int_0^1 \left(\left.\frac{\partial T}{\partial Y}\right|_{Y=+d/2L}\right) dX \tag{14}$$

where q is the heat flux and Q is the heat transfer rate, and the subscripts U and D refer to the upward-facing and downward-facing heated sides of the plate, respectively. The temperature gradients at any heated surface are evaluated by a second-order profile among each wall-node and the next two fluid-nodes. The integrals are approximated by the trapezoid rule.

In addition, the average Nusselt number of the whole plate, Nu, is calculated as the arithmetic mean value of the average Nusselt numbers of any side of the plate, i.e., $(Nu_U + Nu_D)/2$.

Validation of the numerical procedure

Tests on the dependence of the results on the mesh-spacing, as well as on the extent of the computational domain, have been performed for several combinations of values of Ra, φ, and Pr. This has brought to set the grid-spacings and the extents of the integration domain used for computations, which are such that further grid refinements or extensions of the computational domain do not yield for noticeable modifications neither in the heat transfer rates nor in the flow field, that is, the percentage changes of Nu_x and Nu for both sides of the plate and the percentage changes of the maximum value of the velocity component U at X = L/4, L/2 and 3L/4, are smaller than the prescribed accuracy values, i.e., 1% and 2%, respectively.

Typical features of the integration domain are as follows: (a) the number of nodal points lies in the range between 50×100 and 100×400, (b) the extent of the integration domain ranges between 2L and 8L upwards, between L and 3L downwards, and between L and 5L sidewards, depending on Ra, φ, and Pr.

As far as the validation of the numerical code is concerned, reference is made to literature data relevant to plates heated at a single side. For the vertical setting, a comparison between the average Nusselt numbers obtained at different Rayleigh and Prandtl numbers and the corresponding values derived from the Churchill-Chu correlation based on experimental data by other authors [15] and the Raithby-Hollands theoretical equation [16], is reported in Table 1. For the inclined plate, the average Nusselt numbers obtained for air at $Ra = 1.7\times10^6$ are compared with the corresponding values derived by the Hassan-Mohamed correlation based on their experimental data [2], as shown in Tables 2 and 3 for positive and negative inclinations angles, respectively. It may be seen that the Churchill-Chu correlation at low and moderate Rayleigh numbers, as well as the Hassan-Mohamed correlation, underpredict slightly the present Nusselt numbers, whereas the Raithby-Hollands equation tends to over-predict them. However, this was expected, as, at the Rayleigh numbers considered, the Churchill-Chu and Hassan-Mohamed correlations fall slightly below the data upon which they were based, while the predictions of the Raithby-Hollands equation are somewhat higher than several literature experimental data.

In addition, also the velocity distributions – not reported for the sake of brevity – have shown a substantially good degree of agreement with the experimental data by Kierkus [1] for tilting angles in the range between –45deg and +45deg.

Table 1 – Comparison of the present solutions for the average Nusselt number of a vertical plate and literature data

Ra	φ = 0°	Nu		
		Pr = 0.7	7	70
10^2	Present	2.52	2.79	2.88
	Churchill-Chu eqn [15]	2.30	2.62	2.74
	Raithby-Hollands eqn [16]	2.81	3.14	3.28
10^4	Present	5.88	6.68	7.05
	Churchill-Chu eqn [15]	5.81	6.80	7.20
	Raithby-Hollands eqn [16]	6.43	7.43	7.84
10^6	Present	17.47	19.67	20.76
	Churchill-Chu eqn [15]	16.92	20.04	21.30
	Raithby-Hollands eqn [16]	17.55	20.67	21.93

Table 2 – Comparison of the present solutions for the average Nusselt number of a positively inclined plate and the Hassan-Mohamed data

$Ra = 1.7\times10^6$, Pr = 0.7	Nu			
(upper-side heating)	φ = +15°	+30°	+45°	+60°
Present	19.02	18.60	17.82	16.61
Hassan-Mohamed eqn [2]	18.14	17.65	16.78	15.39

Table 3 – Comparison of the present solutions for the average Nusselt number of a negatively inclined plate and the Hassan-Mohamed data

$Ra = 1.7\times10^6$, Pr = 0.7	Nu			
(lower-side heating)	φ = –15°	–30°	–45°	–60°
Present	18.91	18.38	17.46	16.06
Hassan-Mohamed eqn [2]	18.14	17.65	16.78	15.39

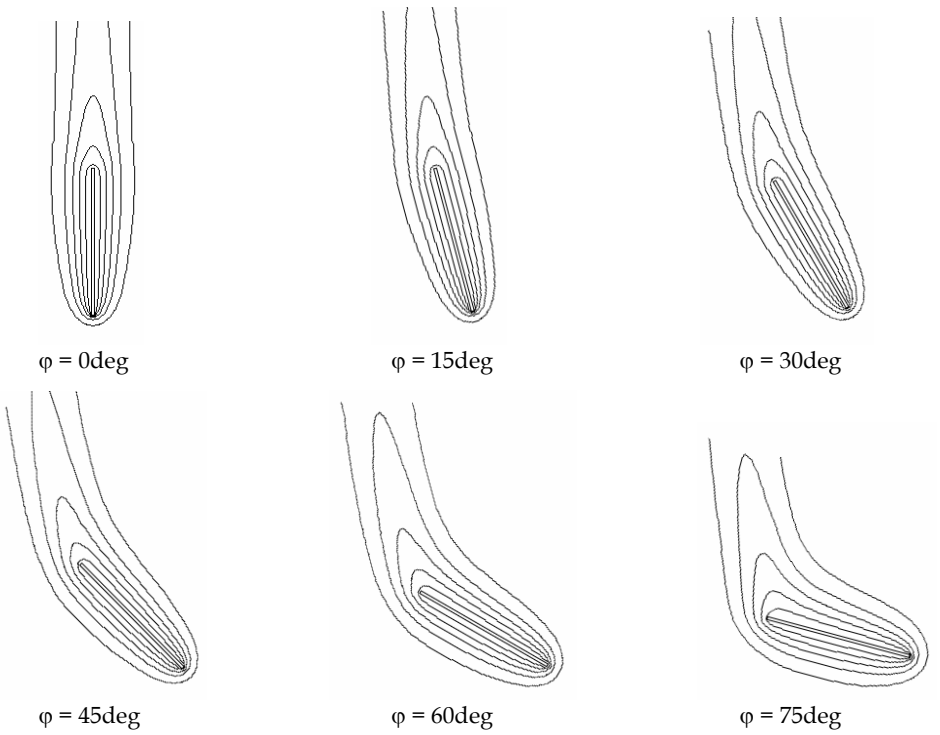

Figure 2 – Effects of the tilting angle: isotherm lines for Ra = 10^4, Pr = 0.7, and φ from 0deg to 75deg step 15deg

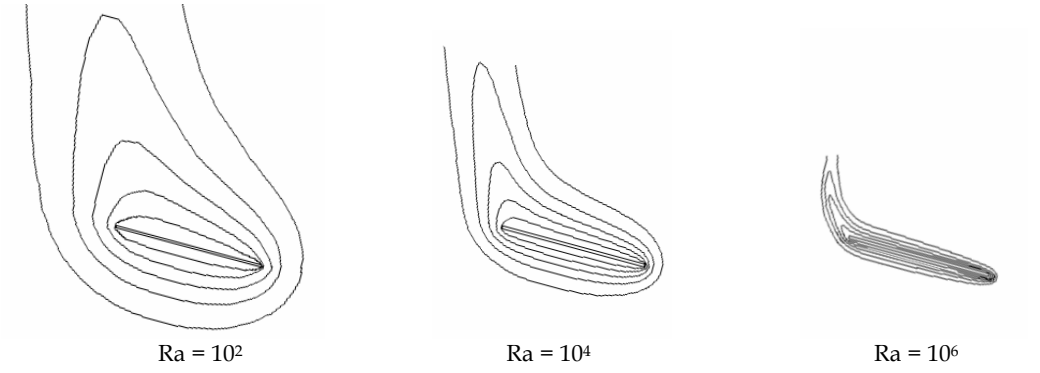

Figure 3 – Effects of the Rayleigh number: isotherm lines for Pr = 0.7, φ = 75deg and Ra = 10^2, 10^4, and 10^6

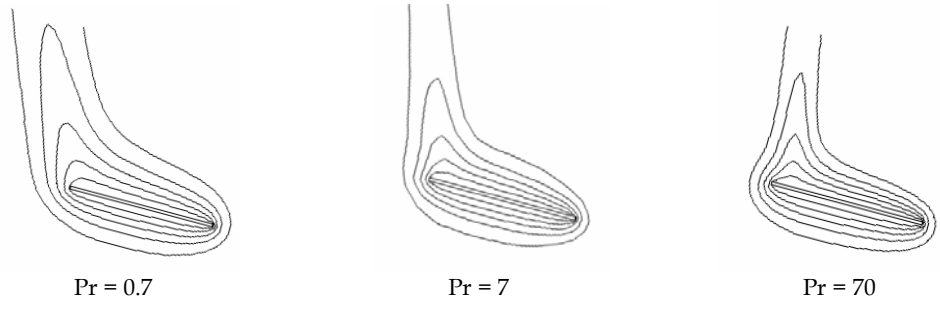

Figure 4 – Effects of the Prandtl number: isotherm lines for Ra = 10^4, φ = 75deg and Pr = 0.7, 7, and 70

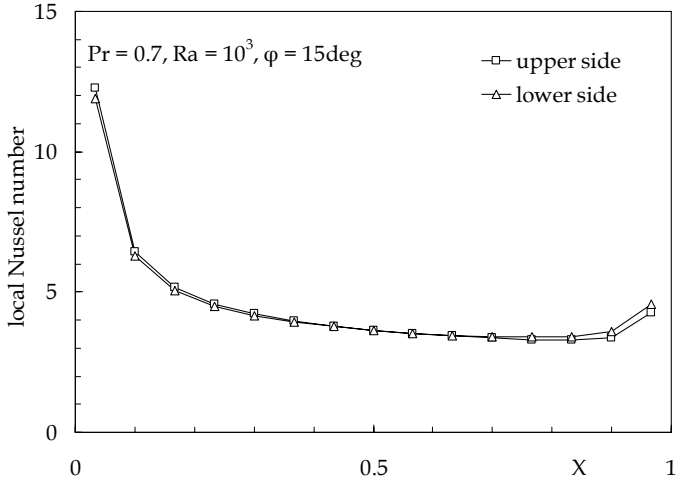

Figure 5 – Distributions of $(Nu_x)_U$ and $(Nu_x)_D$ along the plate for Pr = 0.7, Ra = 10^3, and φ = 15deg

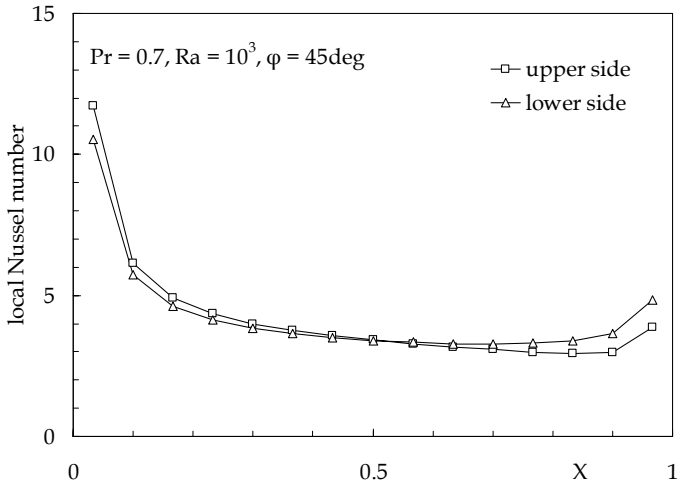

Figure 6 – Distributions of $(Nu_x)_U$ and $(Nu_x)_D$ along the plate for Pr = 0.7, Ra = 10^3, and φ = 45deg

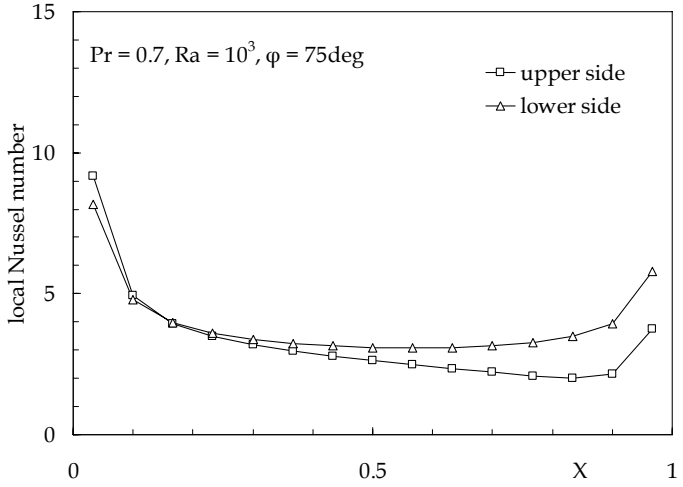

Figure 7 – Distributions of $(Nu_x)_U$ and $(Nu_x)_D$ along the plate for Pr = 0.7, Ra = 10^3, and φ = 75deg

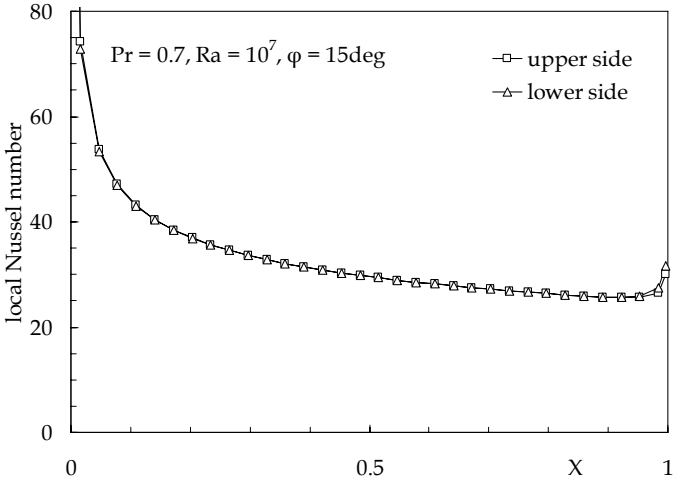

Figure 8 – Distributions of $(Nu_x)_U$ and $(Nu_x)_D$ along the plate for Pr = 0.7, Ra = 10^7, and φ = 15deg

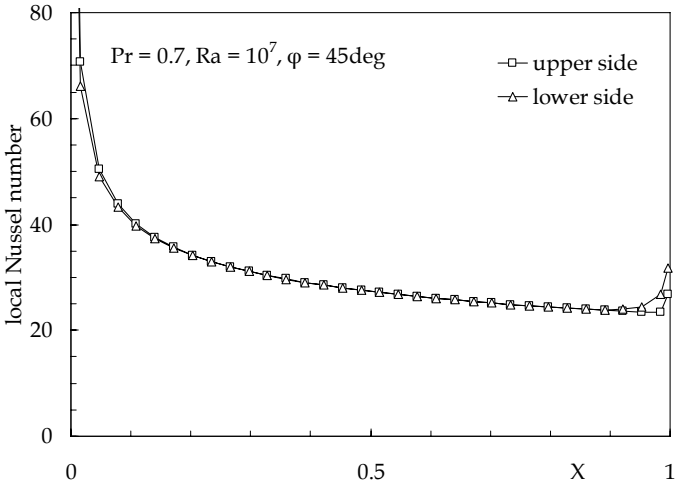

Figure 9 – Distributions of $(Nu_x)_U$ and $(Nu_x)_D$ along the plate for Pr = 0.7, Ra = 10^7, and φ = 45deg

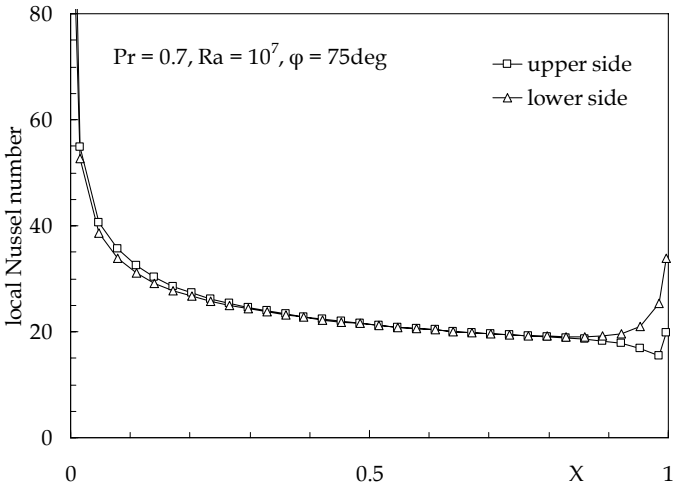

Figure 10 – Distributions of $(Nu_x)_U$ and $(Nu_x)_D$ along the plate for Pr = 0.7, Ra = 10^7, and φ = 75deg

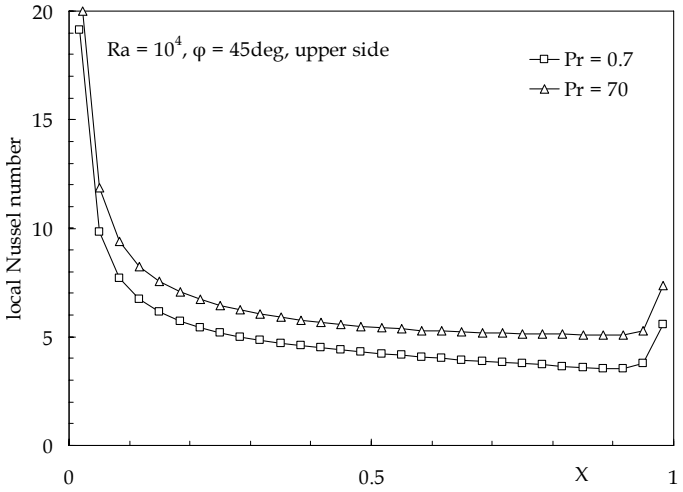

Figure 11 – Distributions of $(Nu_x)_U$ along the plate for Ra = 10^4, φ = 45deg, and different Prandtl numbers (0.7 and 70)

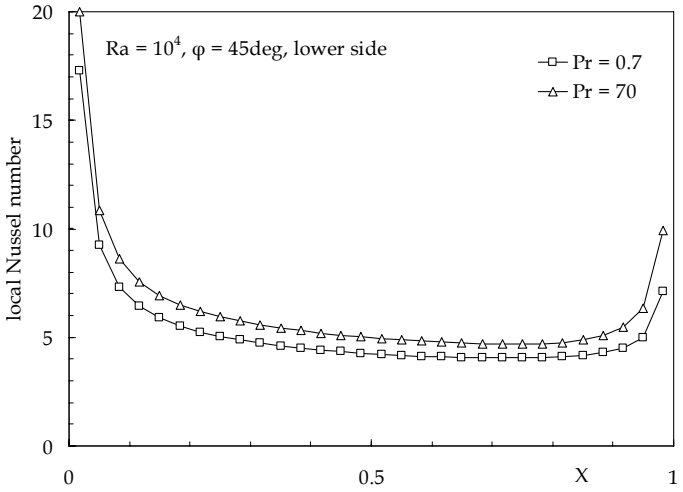

Figure 12 – Distributions of $(Nu_x)_D$ along the plate for Ra = 10^4, φ = 45deg, and different Prandtl numbers (0.7 and 70)

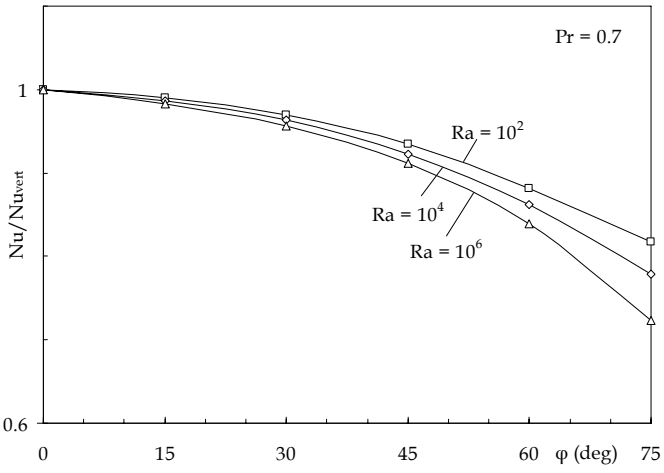

Figure 13 – Distributions of Nu/Nu_{vert} vs. φ (in deg) for Pr = 0.7 and different Rayleigh numbers (10^2, 10^4 and 10^6)

DISCUSSION OF THE RESULTS

Numerical simulations are performed for different values of the Rayleigh number, Ra, in the range between 10^1 and 10^8, the inclination angle, φ, in the range between 0deg and 75deg, and the Prandtl number, Pr, in the range between 0.7 and 70.

Isotherm contours are plotted in Figs. 2–4 for: (a) Ra = 10^4, Pr = 0.7, and φ = 0deg to 75deg; (b) Pr = 0.7, φ = 75deg, and Ra =10^2 to 10^6; and (c) Ra = 10^4, φ = 75deg, and Pr = 0.7 to 70.

It is apparent how the effect of the angle φ is to thicken the plume and decrease its velocity. In addition, for tilting angles above 45deg, the buoyant plume is not anymore rooted in the trailing edge of the plate. As regards the effect of the Rayleigh number, the well-known decrease in thickness of the boundary layer with increasing Ra may be observed, whereas the plume shrinks and rotates slightly outwards; moreover, at large tilting angles, the root of the plume shifts towards the trailing edge of the plate. Finally, as far as the increase of the Prandtl number is concerned, it may be noticed that, owing to the increasing effect of viscosity, the wall jet flowing over the plate is compressed towards the heated surface, thus leading to a shrinking of the plume, which, additionally, rotates inwards.

Of course, the effects discussed above have direct influence upon the local heat fluxes, as shown: (a) in Figs. 5–7, where the distributions of $(Nu_x)_U$ and $(Nu_x)_D$ along the plate for Pr = 0.7, and Ra = 10^3, are reported for φ = 15deg, 45deg, and 75deg; (b) in Figs. 8–10, where the distributions of $(Nu_x)_U$ and $(Nu_x)_D$ along the plate for Pr = 0.7, and Ra = 10^7, are reported for φ = 15deg, 45deg, and 75deg; and (c) in Figs. 11 and 12, where the distributions of $(Nu_x)_U$ and $(Nu_x)_D$ along the plate, respectively, are reported for Ra = 10^4, φ = 45deg, and Pr = 0.7 and 70.

As far as the overall heat transfer performance of the plate is concerned, an overview of the effects of the inclination angle on the amount of heat exchanged is reported in Fig. 13, where the distributions of Nu/Nu_{vert}, i.e., the ratio between the average Nusselt numbers for the inclined plate and for the vertical plate at same Rayleigh and Prandtl numbers, are plotted vs. φ for Pr = 0.7 and Ra = 10^2, 10^4, and 10^6. In accordance with what has been discussed above, it may be seen that the heat transfer rate decreases as the inclination angle of the plate increases, at a rate which increases with both φ, due to the widening of the stagnation region at the upper side of the plate, and Ra.

Moreover, with the scope to highlight in what measure the heat transfer performance of any side of the plate is affected by the simultaneous heating of the opposite side, the distributions of $Nu_x/(Nu_x)_0$, i.e., the ratio between the local Nusselt numbers of any side of the plate for the case of concurrent heating of the opposite side and for the case of perfectly insulated opposite side, are plotted vs. X in Figs. 14–16, where the effects of φ, Ra, and Pr, respectively, are pointed out.

It may be noticed that the effect of the heating of the upper side of the plate on the amount of heat locally transferred at the lower side of the plate is almost neglible, due to the fact that the fluid flow below the plate is promoted mainly by the thermal contribution of its lower side, at least for not too low Rayleigh numbers and leaving aside the proximities of the leading and trailing edges (where a non-negligible increase in the thickness of the boundary layer occurs owing to the upper-side heating).

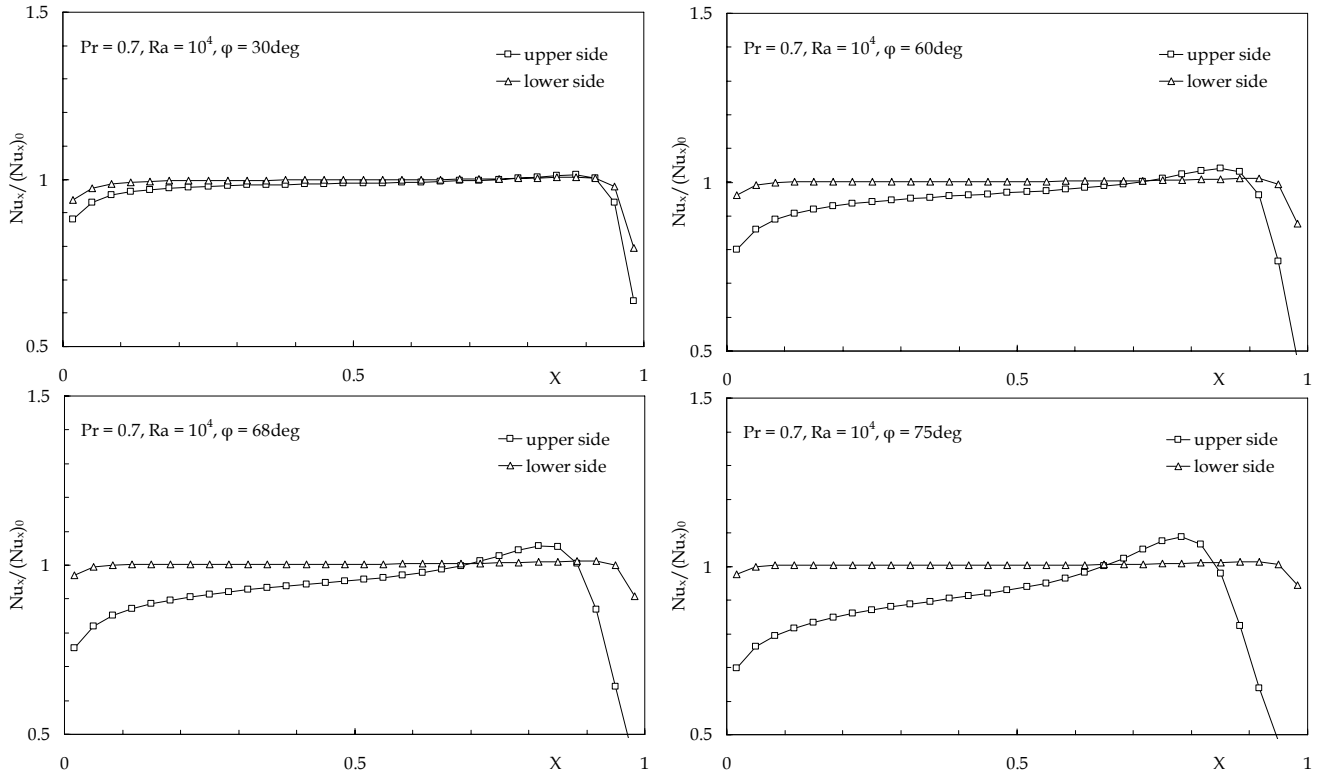

Figure 14 – Distributions of $Nu_x/(Nu_x)_0$ vs. X for Pr = 0.7, Ra = 10^4, and φ = 30deg to 75deg

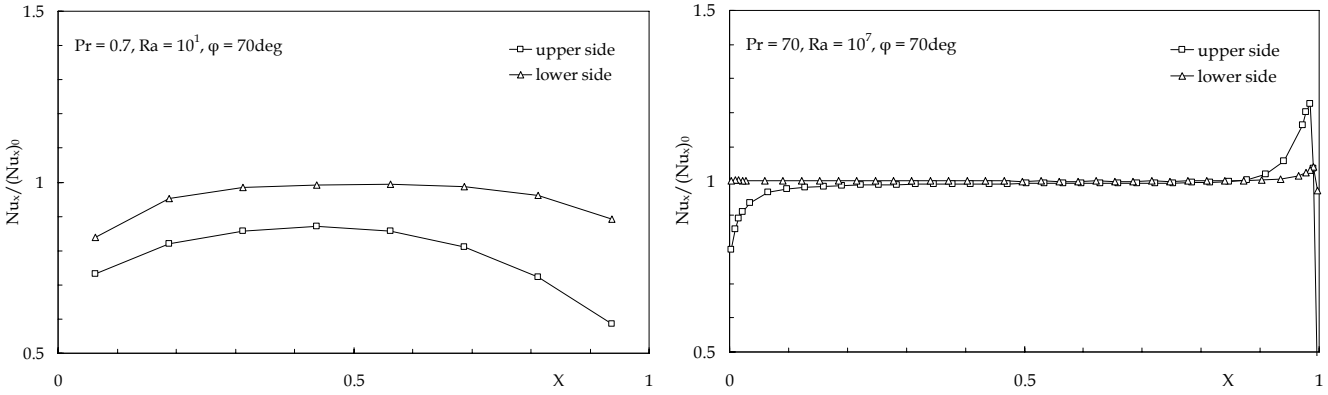

Figure 15 – Distributions of $Nu_x/(Nu_x)_0$ vs. X for Pr = 0.7, φ = 70deg, and Ra = 10^1 and 10^7

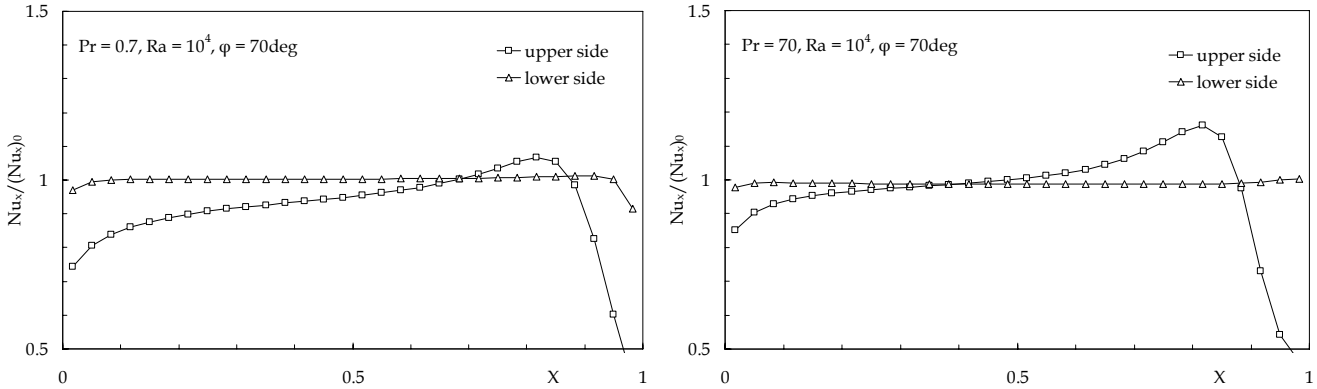

Figure 16 – Distributions of $Nu_x/(Nu_x)_0$ vs. X for Ra = 10^4, φ = 70deg, and Pr = 0.7 and 70

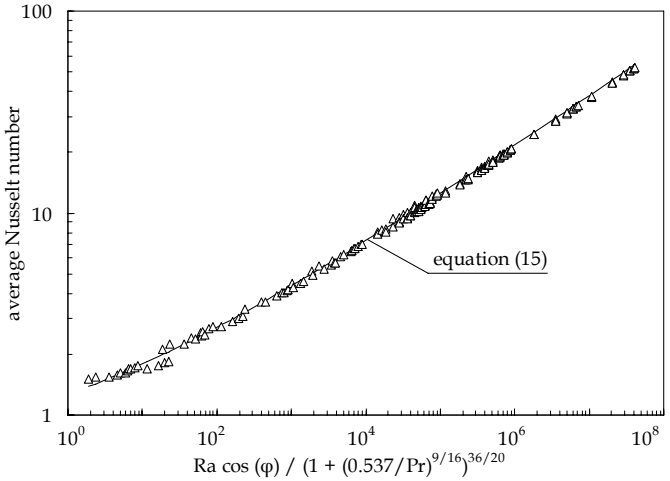

Figure 17 – Correlating equation for the overall heat transfer

In contrast, the effect of the heating of the lower side of the plate on the thermal performance of the upper side is much more significant, at least as long as the orientation of the plate is not too close to the vertical setting. In fact, owing to the heating of its lower side, the whole plate is embedded in an upward-moving convection field whose effect is to decrease the temperature difference between its upper side and the adjacent fluid, and therefore to lessen the local heat transfer. The only exception is represented by the stagnation region, i.e., the region where the plume is rooted, whose thermal performance improves. In fact, owing to the viscous effect of the fluid flow induced by the heating of the lower side of the plate, the plume tends to shrink and get faster. Of course, such enhancement of the relative heat transfer performance becomes higher as the inclination of the plate increases, which is due to the tendency of the stagnation region to widen progressively out (see Fig. 14). A result of the same type is produced also by the increase of the Rayleigh or Prandtl numbers, as a consequence of the faster fluid motion or the larger viscosity effect, respectively (see Figs. 15 and 16).

Finally, the results obtained for the average Nusselt number of the plate may be correlated to the independent variables Ra, φ, and Pr, through the following equation, whose functional structure is directly derived from the expression originally proposed for vertical plates by Churchill and Usagi [17]:

$$\mathrm{Nu} = 0.6 + \frac{0.669}{\left[1 + \left(0.537/\mathrm{Pr}\right)^{9/16}\right]^{9/20}} \left(\mathrm{Ra}\cos\varphi\right)^{0.25} \qquad (15)$$

for $0\mathrm{deg} \le \varphi \le 75\mathrm{deg}$, $10^1 \le \mathrm{Ra} \le 10^8$, and $0.7 \le \mathrm{Pr} \le 70$, with a 2.9% standard deviation of error, and error ranges of ±9% and ±5%, with levels of confidence of 100% and 92%, respectively, as shown in Fig. 17.

CONCLUSIONS

Steady natural convection from tilted thin plates with both sides heated at uniform temperature, is studied numerically for the laminar regime. A SIMPLE-C algorithm has been used for the solution of the mass, momentum, and energy governing equations. Simulations have been performed for tilting angles of the plate from 0deg to 75deg, Rayleigh numbers from 10^1 to 10^8, and Prandtl numbers from 0.7 to 70. The heating at a single side, the other being adiabatic, has also been considered.

It has been found that the heat transfer performance of the whole plate heated at both sides increases as the Rayleigh and Prandtl numbers increase, while decreases as the tilting angle of the plate increases, at a rate which increases with φ and Ra.

In addition, the heat transfer performance of the lower side of the plate is practically independent of the thermal boundary condition imposed at the opposite side of the plate, i.e., heated at same temperature or adiabatic. On the contrary, the amount of heat exchanged at the upper side of the plate decreases when the opposite lower side is heated rather than insulated, with the only exception of the stagnation region, i.e., the region where the plume is rooted, whose relative heat transfer performance increases with increasing φ, Ra and Pr.

Finally, a dimensionless correlation of the Churchill-Usagi type has also been developed for the heat transfer performance of the whole plate.

However, due to the assumption of steady, two-dimensional laminar flow, the present paper should be regarded as a first-stage paper on the subject, which deserves further investigation in order to take into account the influence of three-dimensional effects, e.g., unsteady longitudinal rolls, which in a 2D study are necessarily neglected.

NOMENCLATURE

d	thickness of the plate
g	gravity vector
g	gravitational acceleration
k	thermal conductivity of the fluid
L	length of the plate
Nu_x	local Nusselt number = $qL/k(t_p - t_\infty)$
Nu	average Nusselt number = $Q/k(t_p - t_\infty)$
p	dimensionless pressure
Pr	Prandtl number = ν/α
Q	heat transfer rate
q	heat flux
Ra	Rayleigh number = $g\beta(t_p - t_\infty)L^3\mathrm{Pr}/\nu^2$
T	dimensionless temperature
t	temperature
U	dimensionless X-wise velocity component
V	dimensionless velocity vector
V	dimensionless Y-wise velocity component
X	dimensionless coordinate parallel to the plate
x	coordinate parallel to the plate
Y	dimensionless coordinate normal to the plate
y	coordinate normal to the plate

Greek symbols

α	thermal diffusivity of the fluid
β	coefficient of volumetric thermal expansion of the fluid
φ	tilting angle of the plate with respect to gravity
ν	kinematic viscosity of the fluid
ρ	density of the fluid

Subscripts

D	downward-facing surface, lower side of the plate
p	plate surface
U	upward-facing surface, upper side of the plate
0	relevant to the case of opposite side perfectly insulated
∞	undisturbed fluid

REFERENCES

[1] W. T. Kierkus, An analysis of laminar free convection flow and heat transfer about an inclined isothermal plate, Int. J. Heat Mass Transfer 11 (1968) 241-253.

[2] K. E. Hassan, S. A. Mohamed, Natural convection from isothermal flat surfaces, Int. J. Heat Mass Transfer 13 (1970) 1873-1886.

[3] T. Fujii, H. Imura, Natural convection heat transfer from a plate with arbitrary inclination, Int. J. Heat Mass Transfer 15 (1972) 755-767.

[4] M. Al-Arabi, B. Sakr, Natural convection heat transfer from inclined isothermal plates, Int. J. Heat Mass Transfer 31 (1988) 559-566.

[5] G. C. Vliet, Natural convection local heat transfer on constant-heat-flux inclined surfaces, J. Heat Transfer 91 (1969) 511-516.

[6] G. C. Vliet, D. C. Ross, Turbulent natural convection on upward and downward facing inclined constant heat flux surfaces, J. Heat Transfer 97 (1975) 549-555.

[7] D. E. Fussey, I. P. Warneford, Free convection from a downward facing inclined flat plate, Int. J. Heat Mass Transfer 21 (1978) 119-126.

[8] H. Shaukatullah, B. Gebhart, An experimental investigation of natural convection flow on an inclined surface, Int. J. Heat Mass Transfer 21 (1978) 1481-1490.

[9] J. A. King, D. D. Reible, Laminar natural convection heat transfer from inclined surfaces, Int. J. Heat Mass Transfer 34 (1991) 1901-1904.

[10] M. M. Hasan, R. Eichhorn, Local nonsimilarity solution of free convection flow and heat transfer on an inclined isothermal plate, J. Heat Transfer 101 (1979) 642-647.

[11] T. S. Chen, H. C. Tien, B. F. Armaly, Natural convection on horizontal, inclined, and vertical plates with variable surface temperature or heat flux, Int. J. Heat Mass Transfer 29 (1986) 1465-1478.

[12] J. J. Wei, B. Yu, H.S. Wang, W. Q. Tao, Numerical study of simultaneous natural convection heat transfer from both surfaces of a uniformly heated thin plate with arbitrary inclination, Heat Mass Transfer 38 (2002) 309-317.

[13] J. P. Van Doormaal and G. D. Raithby, Enhancements of the simple method for predicting incompressible fluid flows, Numer. Heat Transfer 11 (1984) 147-163.

[14] B. P. Leonard, A stable and accurate convective modelling procedure based on quadratic upstream interpolation, Comp. Meth. in Appl. Mech. Engng. 19 (1979) 59-78.

[15] S. W. Churchill, H. H. Chu, Correlating equations for laminar and turbulent free convection from a vertical plate, Int. J. Heat Mass Transfer 18 (1975) 1323-1329.

[16] G. D. Raithby, K. G. T. Hollands, Laminar and turbulent free convection from elliptic cylinders, with a vertical plate and horizontal circular cylinder as special case, J. Heat Transfer 98 (1976) 72-80.

[17] S. W. Churchill, R. Usagi, A general expression for the correlation of rates of transfer and other phenomena, A.I.Ch.E. Journal 18 (1972) 1121-1128.